Encyclopedia of Earthquake Engineering
DOI 10.1007/978-3-642-36197-5_378-1

Passive Seismic Interferometry for Subsurface Imaging

Deyan Draganov[a]* and Elmer Ruigrok[b]
[a]Department of Geoscience and Engineering, Delft University of Technology, Delft, The Netherlands
[b]Department of Earth Sciences, Utrecht University, Utrecht, The Netherlands

Synonyms

Ambient noise; Body waves; Cross-correlation; Green's function retrieval; Reflection imaging; Reflections; Seismic interferometry; Teleseismic arrivals

Introduction

Seismic interferometry is a method that allows the retrieval of the seismic response at one receiver from a virtual source at the position of another receiver. The method was first proposed in the seismic exploration community by Claerbout (1968) for a horizontally layered subsurface. The author showed that by autocorrelating the transmission response recorded at a receiver at the Earth's surface from noise sources in the subsurface, one would retrieve the reflection response at this receiver from a virtual source also at that location. In the following decades, the applications of this idea were rare (Scherbaum 1987; Duvall et al. 1993; Daneshvar et al. 1995). But from the turn of the century, the fortunes changed and the method rapidly gained in popularity. This happened in the seismological community, due to applications to earthquake coda waves (Campillo and Paul 2003) and ambient noise (Shapiro and Campillo 2004), and in the exploration seismic community, due to the development of a solid theory for 3D media (Wapenaar 2004) and proposal to use the method also with controlled sources (Schuster et al. 2004).

Lately, the method of seismic interferometry has found different applications, like in imaging of the subsurface, monitoring of changes in the subsurface, quality-factor estimation, suppression of surface waves, etc., at different scales with different types of sources. Overviews can be found in Wapenaar et al. (2008) and Schuster (2009).

When the goal is to obtain an image of the subsurface with relatively high resolution, the most frequently applied method is reflection seismics with artificial sources at the surface, as is standard in the exploration seismology. It is not always possible, though, to use artificial sources, due to environmental or safety considerations, for example. Besides artificial sources, also so-called passive sources are used. Any source that is not designed and controlled specifically for the seismic experiment could be referred to as being passive. This could be, e.g., a highway, a pumping unit, induced seismicity, or a significant earthquake. When artificial sources cannot be applied, passive seismic interferometry can be used to retrieve the reflection response of the subsurface under an array of receivers. The retrieved reflection response is than to be used in a standard exploration seismic processing flow for obtaining an image of the subsurface (for processing, see, e.g., Yilmaz 1999). Passive seismic interferometry can be applied to recordings from transient sources or ambient noise. Often, the responses from transient sources can be recorded separately. Such could be recordings from distant seismicity (relative to the imaging target). When separate recordings cannot be obtained, the data should be treated as ambient noise and processed accordingly.

*Email: d.s.draganov@tudelft.nl

Encyclopedia of Earthquake Engineering
DOI 10.1007/978-3-642-36197-5_378-1

This reference is about retrieval of body-wave reflections from passive sources and is built up as follows. In the next section, the basic seismic-interferometry relation is discussed for receivers at the Earth's surface and illumination from below. In section "Toward Application," this relation is adjusted for passive seismics, and a general processing flow is presented. The required input for seismic interferometry is either waves induced by local sources that travel or are scattered upward, or waves from distant seismicity that initially propagate downward, but bend upward before reaching the receivers. The waves from these two origins have different characteristics and hence require different treatment. In section "Imaging Using Distant Seismicity," the theory is implemented into a processing flow for retrieving reflections from distant seismicity. In section "Imaging Using Local Seismicity and Ambient Noise," the processing flow is adapted for local seismicity and noise fields. For both applications, examples are discussed.

Theory

For an elastic lossless medium, the retrieval of the Green's function $G^{v,f}_{p,q}(\mathbf{x}_B, \mathbf{x}_A, t)$ between two receivers at positions $\mathbf{x}_A$ and $\mathbf{x}_B$, representing a particle-velocity measurement in the x_p direction at $\mathbf{x}_B$ as if a virtual force source f is present at $\mathbf{x}_A$ and acting in the x_q direction, can be formulated as (Wapenaar and Fokkema 2006)

$$G^{v,f}_{p,q}(\mathbf{x}_B, \mathbf{x}_A, t) + G^{v,f}_{p,q}(\mathbf{x}_B, \mathbf{x}_A, -t) \approx \frac{2}{\rho c^K} \int_{\partial D_1} G^{v,\phi}_{p,K}(\mathbf{x}_B, \mathbf{x}, t) * G^{v,\phi}_{q,K}(\mathbf{x}_A, \mathbf{x}, -t) d^2\mathbf{x}. \quad (1)$$

In the above equation, $G^{v,\phi}_{p,K}(\mathbf{x}_B, \mathbf{x}, t)$ and $G^{v,\phi}_{p,K}(\mathbf{x}_A, \mathbf{x}, t)$ are the measured Green's functions at the two receivers from impulsive P- or S-wave sources (for ϕ exchanged with P or S, respectively) at positions $\mathbf{x}$ along a boundary ∂D_1 that effectively encloses the receivers (Fig. 1). The repeated uppercase Latin subscript $_K$ takes on the values 0, 1, 2, and 3 and represents a summation from 0 to 3. This means that at each point on ∂D_1, there is a P-wave source and S-wave sources in three perpendicular directions and that

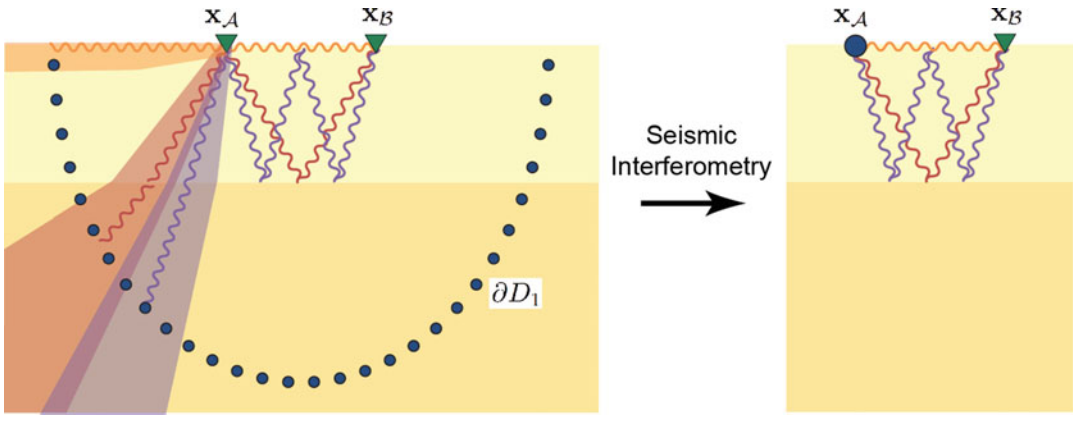

Fig. 1 Cartoon illustrating the input (*left*) and output (*right*) of seismic interferometry, for a layer (*light yellow*) over a half-space (*dark yellow*) model. Two receivers on the Earth's surface (*green triangles*) record the wavefields induced by subsurface sources (*blue dots*). After applying seismic interferometry, the response is obtained as if there were a source at $\mathbf{x}_A$ and a receiver at $\mathbf{x}_B$. The *wiggled lines* depict different events in the original responses (*left*) that contribute to events in the retrieved response (*right*). The *fan-shaped* areas represent the stationary-phase regions for the different contributions. This figure is an adaptation from a similar figure in Wapenaar and Fokkema (2006), which shows sources contributing to the retrieval of body waves from a point scatterer

DOI 10.1007/978-3-642-36197-5_378-1

the receivers record separate responses from each of these sources. The symbols ρ and c^K are the constant density and seismic wave velocity along ∂D_1, where $c^K = c_P$ (for $K = 0$) and $c^K = c_S$ (for $K = 1$, 2, or 3) are the P- and S-wave velocities, respectively. The $*$ sign denotes convolution, but because one of the quantities in the right-hand side is reversed in time, the operation is equivalent to correlation. Equation 1 is an approximation of the exact formulation (see Eq. 19 in Wapenaar and Fokkema 2006) to make it suitable for field applications. To obtain this approximate relation, the following assumptions are made:

- The boundary sources are in the far field of the receivers.
- The medium outside the enclosing boundary is not causing scattering that reaches the receivers.
- The medium parameters (density and velocity) across the enclosing boundary change smoothly.
- The density and velocity along the enclosing boundary are constant.

When the above assumptions are fulfilled, for example, when the source boundary is a half sphere with a very large radius, the retrieved Green's function will have both its amplitudes and travel times correct. When not all of the assumptions are fulfilled, only the travel times would be correct.

The contribution to the events in the retrieved Green's function does not come from the complete source boundary, but only from sources inside the stationary-phase region (Snieder 2004). This is the region along the ray (fan-shaped areas in Fig. 1), which, for reflected waves, goes from the source boundary to the receiver at $\mathbf{x}_A$, reflects at the Earth's surface, and after reflecting from a target reflector is recorded at $\mathbf{x}_B$. Physically, the correlation process removes the travel path from the source boundary to $\mathbf{x}_A$ and retains the reflection travel path between $\mathbf{x}_A$ and $\mathbf{x}_B$. With sources only in the stationary-phase areas, and with the sources much more irregularly distributed than on the ideal semicircle in Fig. 1, the desired reflection events are still retrieved correctly. This allows implementation of the interferometric integral to natural seismicity.

Toward Application

Equation 1 is not practical for direct implementation to naturally induced wavefields. First, the $\frac{1}{\rho c^K}$ factor in the right-hand side is dropped, because the medium parameters along the enclosing boundary are generally not known. Moreover, the sum over different source components is omitted. The different source components need to be induced and recorded separately or decomposed from the recording. This is often not feasible. Furthermore, the continuous integral is approximated with a sum over (irregularly spaced) source locations. Hence, seismic interferometry is directly applied to the physical measurements according to

$$G^{v,f}_{p,q}(\mathbf{x}_B, \mathbf{x}_A, t) + G^{v,f}_{p,q}(\mathbf{x}_B, \mathbf{x}_A, -t) \approx \sum_{i=1}^{n} G^{v}_{p}(\mathbf{x}_B, \mathbf{x}^i, t) * G^{v}_{q}(\mathbf{x}_A, \mathbf{x}^i, -t)\Delta^2\mathbf{x}^i, \tag{2}$$

where i is a source index, n is the total amount of sources, and $G^v_p(\mathbf{x}_B, \mathbf{x}^i, t)$ and $G^v_q(\mathbf{x}_A, \mathbf{x}^i, t)$ are the responses of single- or mixed-source types. $\Delta^2\mathbf{x}^i$ denotes the area represented by a single source. Omission of the sum over source components leads to nonphysical (ghost) events related to conversions not being canceled entirely.

As mentioned above, the theory of seismic interferometry by cross-correlation is derived for a lossless medium. When the waves experience intrinsic losses in the medium, the result retrieved by seismic

DOI 10.1007/978-3-642-36197-5_378-1

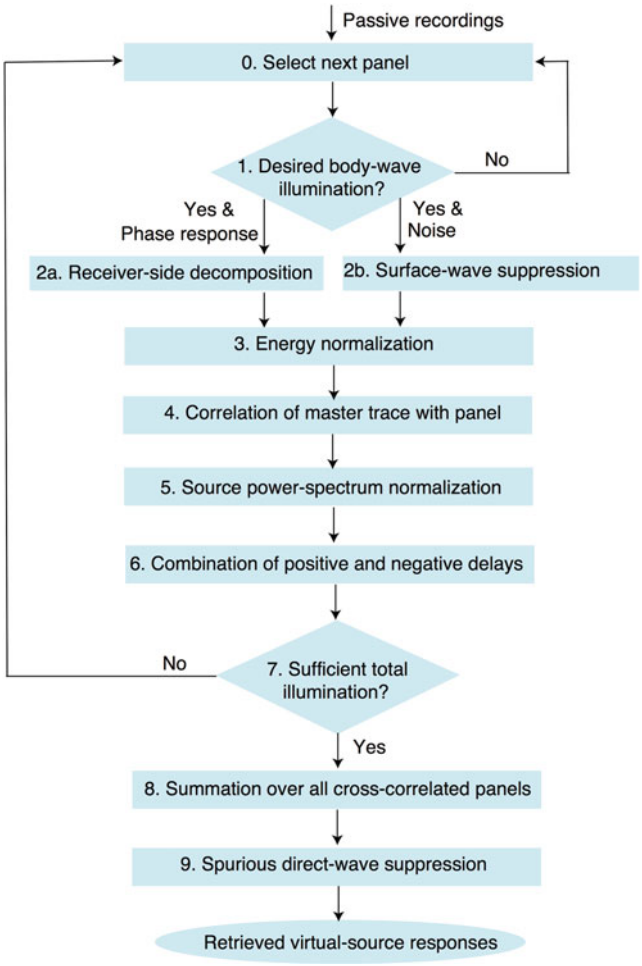

Fig. 2 Flowchart summarizing the procedure for retrieval of body-wave reflections using passive seismic interferometry. Panel describes a recording from a separate seismic source or a time window from recorded noise

interferometry by cross-correlation might contain additional ghost arrivals due to the losses (e.g., Draganov et al. 2010).

The procedure for retrieval of reflections with passive seismic interferometry is explained below and summarized in the flowchart in Fig. 2.

Imaging Using Distant Seismicity

The basic equation describing seismic interferometry with transient sources is derived from Eq. 2:

$$\left\{G^{v,f}_{p,q}(\mathbf{x}_B,\mathbf{x}_A,t)+G^{v,f}_{p,q}(\mathbf{x}_B,\mathbf{x}_A,-t)\right\}*S_0(t)\approx\sum_{i=1}^{n}v_p\left(\mathbf{x}_B,\mathbf{x}^i,t\right)*v_q\left(\mathbf{x}_A,\mathbf{x}^i,-t\right)*F(t)\Delta^2\mathbf{x}^i, \quad (3)$$

where $v_p(\mathbf{x}_B,\mathbf{x}^i,t)=G^v_p(\mathbf{x}_B,\mathbf{x}^i,t)*s^i(t)$ is the measured particle velocity at the surface, $s^i(t)$ is the source function of the seismic source at position $\mathbf{x}^i$, n is the total amount of sources, and i is a source index. $F(t)$ is a shaping filter that deconvolves for $S(t)=s^i(t)*s^i(-t)$ and convolves the result with a desired wavelet $S_0(t)$.

DOI 10.1007/978-3-642-36197-5_378-1

As mentioned in the previous section, the boundary sources should effectively enclose the receivers. Only in such a case the complete Green's function could be retrieved. When the aim is to obtain an image of the subsurface reflectors, there is no need to retrieve surface waves, but only body-wave reflections. Using stationary-phase analysis, it can be shown that source at or close to the surface would mainly contribute to the retrieval of surface waves (see, e.g., the horizontal wiggle line in Fig. 1), while body-wave reflections would be retrieved from sources below the target region or from sources for which a part of the wavefield reflects or refracts below the target region. An effective illumination from below is reached with distant seismicity (Abe et al. 2007; Ruigrok et al. 2010; Frank et al. 2014). For applications with seismic interferometry, seismicity is defined as distant when it allows for separation of the P- and S-phases using time windowing. This is, for example, achieved for teleseismic arrivals.

The earthquakes occur infrequently in time, so the longer the measurement, the larger the number of earthquakes that can be used for retrieval of reflections. The earthquakes are also very sparsely distributed in space, mainly occurring in specific areas (e.g., the Ring of Fire in the Pacific Ocean). Because of this, the illumination of the receiver array from the seismic sources would be limited. To retrieve the complete reflection response, all stationary-phase regions that contribute to retrieval of reflections should be sampled by sources. Describing the illumination of the receiver array from the available boundary sources in terms of ray parameter and back azimuth means to know which parts of the Green's function (reflection response) could possibly be retrieved. The illumination analysis is step 1 in the flowchart (Fig. 2). A multichannel recording from a seismic source is termed a panel in Fig. 2. The illumination analysis is performed per panel.

Implementing Eq. 3 without decomposition yields Green's functions that contain both P- and S-wave reflections. For the subsequent imaging, it is desirable to obtain only one wave type at the source and only one at the receiver. For distant seismicity, P- and S-wave phases arrive at different times, due to the long propagation paths. Thus, source-side decomposition can be implemented by simply time windowing either P- or S-wave phases. When the array is small with respect to the distance to the source, a significant part of the energy in one phase response has the same ray parameter. Knowing near-surface velocities, this allows receiver-side decomposition of the wavefield measured in north N, east E, and vertical Z directions into compressional P-, shear vertical SV-, and shear horizontal SH-waves (step 2a in Fig. 2); see Kennett (1991).

The different seismic sources in the dataset would have different strength. Because of this, in the summation process in Eq. 3, some of the correlated panels might be much stronger (even orders stronger) than others. This would effectively result in lowering the number of available seismic sources. To overcome this, each panel is normalized by its energy (step 3 in Fig. 2).

After the normalization, the separate panels are ready for correlation. A trace is chosen at the position of a receiver where a virtual source is to be retrieved (position $\mathbf{x}_A$ in Eq. 3). Such a trace is termed master trace in Fig. 2. The master trace is correlated with the panel, from which it is extracted (step 4 in Fig. 2).

As a preparation for summation of the cross-correlation results, the power spectra need to be equalized (step 5 in Fig. 2). Note that in Eq. 3 it is assumed that the autocorrelation of the different seismic sources is equal. This can be achieved by estimating and deconvolving the source time functions (step 5 in Fig. 2), and if desired, the deconvolved result could be convolved with a specific wavelet for ease of interpretation (e.g., Ricker wavelet). In Eq. 3, the deconvolution and convolution are described with the shaping filter $F(t)$. When the source time functions are unknown, equalization can be achieved by frequency band-pass filtering and whitening. To circumvent spurious events created by the whitening procedure, the chosen band should not exceed the range where each of the sources has signal. The whitening can be applied with a running-absolute-mean normalization in the frequency domain, to soften, but still retain the peaks and notches in the amplitude spectra.

DOI 10.1007/978-3-642-36197-5_378-1

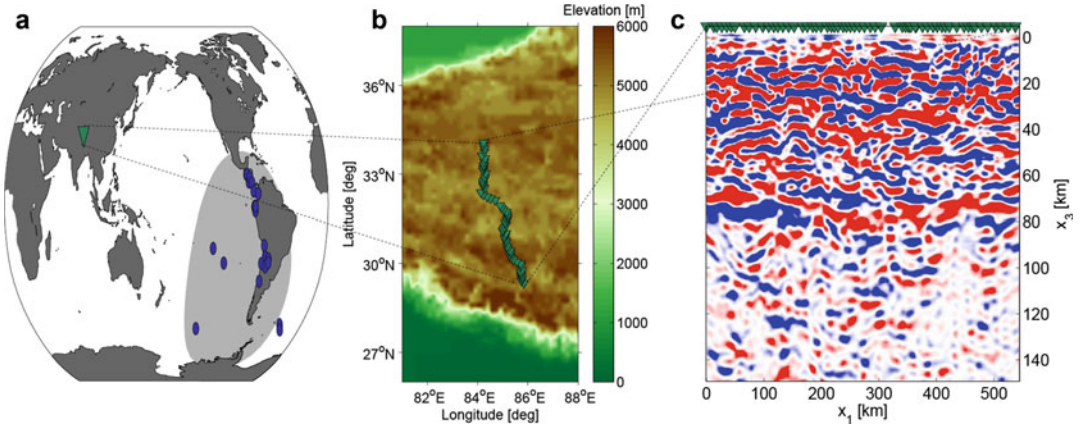

Fig. 3 (**a**) The source distribution (*blue dots*) and the location of the Hi-CLIMB experiment (*green triangle*), (**b**) the layout of the used receivers (*green triangles*), and (**c**) the resulting reflectivity image of the subsurface below the array after applying seismic interferometry and imaging. $x_1 = 0$ corresponds with the southernmost receiver. On the image, *red* and *blue* denote positive and negative impedance contrasts, respectively. The effective wavelet is similar to a Ricker wavelet. Hence, a sudden increase in seismic impedance with depth is imaged with *red*, with *blue* side lobes on either side (Adapted from Ruigrok and Wapenaar (2012))

Equation 3 states that when the receiver array is illuminated from all directions (the source boundary effectively encloses the receivers), the complete Green's function would be retrieved at positive and negative times. In practice, the illumination will not be from all directions, so parts of the Green's function might happen to be retrieved only at negative times, while other parts only at positive times. Knowing the specific illumination of the array from the available seismic sources allows to at least partly remedy this problem and obtain a more complete retrieved Green's function. For a correlated panel, depending on the specific ray parameter of illumination and the position of the master trace, the positive times to one side of the master trace are combined (concatenated) with the time-reversed negative times on the other side of the master trace (Ruigrok et al. 2010; Draganov et al. 2013). This is step 6 in Fig. 2.

The above six processing steps are repeated until cross-correlated panels for a sufficient illumination range have been obtained. Subsequently, the cross-correlated panels are summed together (step 8 in Fig. 2) to give a nearly final virtual common-source gather for a virtual source at the position of the chosen master trace.

When the steps 1–7 in Fig. 2 are repeated for a master trace at all receiver positions, virtual common-source gathers are retrieved for virtual sources along the complete receiver array.

Not including illumination from large ray parameters (sources near the surface in Fig. 1) prevents the retrieval of direct waves. Yet, the incompleteness of the integration surface leads to edge effects. The most severe one is related to the cross-correlation of the strongest arrival. This event can be directly muted or estimated using common-offset gathers and then removed from the retrieved data (Ruigrok and Wapenaar, 2012).

After suppression of this edge effect (step 9 in Fig. 2), the obtained responses can be processed to obtain an image of the subsurface reflectors.

Figure 3 shows the results of applying the above workflow to data from the Hi-CLIMB experiment (2002–2005). One part of the experiment's geometry was a nearly linear transect of stations crossing a large part of the Tibetan Plateau (Fig. 3b). At teleseismic distances, there was insufficient surface distribution of earthquakes to retrieve reflections between all the station positions by summing cross-correlations (Eq. 3 for $\mathbf{x}_B \neq \mathbf{x}_A$). However, there was enough illumination to retrieve reflections as if there were both a source and a receiver at each receiver position. These so-called zero-offset reflection

DOI 10.1007/978-3-642-36197-5_378-1

responses were obtained by implementing Eq. 3 for $\mathbf{x}_B = \mathbf{x}_A$. First, earthquakes were selected in a zone at the other side of the globe (gray-shaded zone on Fig. 3a) for which the direct waves traversed the core. These so-called global phases illuminated the subsurface below the receivers with small angles of incidence. Next, from the total response, time windows around the global phases were taken, autocorrelated, source power spectrum normalized, and stacked. Subsequently, the spurious direct wave was suppressed. The used time windows included the reverberations from contrasts near the receiver array and near the sources. Stacking over sufficiently many (>10) earthquake responses was necessary to both sample the stationary-phase areas for body-wave reflections (Fig. 1) and to stack out source-side reverberations. To the resulting reflection responses, multiple suppression, projection to a line, migration, and time-to-depth conversion were applied (see Yilmaz 1999 for processing) to obtain the image shown in Fig. 3c. This image contains a region with high reflectivity (the crust) at the top and a region with much less reflectivity (the upper mantle) below. The undulating reflector (the Moho) at ~75 km depth separates the two zones.

Imaging Using Local Seismicity and Ambient Noise

Recordings of ambient noise allow a less deterministic implementation than distant seismicity. The same is the case when using local seismicity, but sometimes even regional seismicity. In the case of local or regional seismicity, the different body-wave phases (P- and S-wave arrivals) cannot be separated well in time and interpreted unambiguously, as is the case with distant seismicity. This means that they should be used for seismic interferometry in the same way ambient noise is used. Recordings of ambient noise can be due to both local and distant sources. Even when only distant noise sources are active, the different phases still cannot be separated in time. The semicontinuous nature of the noise source causes different phases to arrive simultaneously at the receivers. Besides, multiple noise sources could be active at the same time.

When the aim is to obtain a subsurface image from ambient noise, receivers are planted at the desired positions and set to record for certain time period – hours, days, months, or even years. The recorded, possibly continuous, noise is processed by separating it into time windows (panels), which could or could not be overlapping in time. The seismic-interferometry relation to be used is

$$\left\{ G^{v,f}_{p,q}(\mathbf{x}_B, \mathbf{x}_A, t) + G^{v,f}_{p,q}(\mathbf{x}_B, \mathbf{x}_A, -t) \right\} * S_0(t) \approx \sum_{i=1}^{n} v^i_p(\mathbf{x}_B, t) * v^i_q(\mathbf{x}_A, -t) * F(t), \tag{4}$$

where $v^i_p(\mathbf{x}_B, t)$ is one of the available i noise panels recorded at the receiver at position $\mathbf{x}_B$, while now $F(t)$ is a shaping filter that deconvolves the term inside the summation sign for the autocorrelation of the recorded noise in panel i. Formally, Eq. 4 can be derived from Eq. 3 by taking the boundary sources to be noise sources emitting uncorrelated noise and acting simultaneously (Wapenaar and Fokkema, 2006, Eq. 86) or transient sources acting sequentially. Wapenaar and Fokkema (2006) use an ensemble average over different noise realizations. In practice, the ensemble average is exchanged for summation over relatively long time recordings, thus obtaining Eq. 4. The relatively long recordings are required to assure that the recorded noise is uncorrelated. When using local seismicity as an input to Eq. 4, panels with the duration of the earthquake responses are taken. Typically, one such earthquake panel is much shorter than an ambient noise panel.

It is shown that the retrieval of the reflection response of the subsurface from ambient noise requires the presence of body waves in the recorded noise (Draganov et al. 2009, Ruigrok et al. 2011). As Eq. 4 follows from Eq. 3, also for noise sources is true what was concluded from stationary-phase analysis for

DOI 10.1007/978-3-642-36197-5_378-1

Eq. 3 – that sources close to the surface would mainly generate surface waves and thus would contribute to the retrieval of surface waves and that the retrieval of reflections comes from relatively deeper sources that generate body waves or from distant sources for which a part of the wavefield reflects or refracts below the target region. This also dictates the practical need for long recordings, as the noise sources of body waves do not act simultaneously, but would be active at different time instances. Thus, the longer the recordings, the bigger the chance that illumination from the required stationary-phase zones is captured.

By cross-correlating free-surface multiple reflections, a reflection response of the subsurface could be retrieved also from noise sources at the surface (Nakata et al. 2011). In their article, the authors use the anthropogenic noise generated by transport traffic along roads and railways. The coherence process whitens the spectrum of the noise panels and thus brings forward the weak body-wave energy present in the noise. It also deconvolves for the noise function of the sources. But care should be taken when interpreting results from seismic interferometry applied to recordings from surface sources. In such cases, when the surface sources are relatively close to the receiver array, so-called one-sided illumination is present, and nonphysical reflections would be retrieved (Snieder et al. 2006; Draganov et al. 2012; King and Curtis 2012). These arrivals might be misinterpreted for physical reflections. Because of this, it would be better to retrieve reflections from subsurface sources or from relatively distant surface sources.

The body waves in the recorded noise could result from local and regional seismicity (Panea et al. 2014, Nakata et al. 2014), but also from ocean swell (microseism noise) or wind seas (Ruigrok et al. 2011). The distant noise sources provide, among others, diving waves that illuminate the target region from below.

The processing flow for retrieving of reflections from ambient noise is nearly the same as the one for distant seismicity, but for the following differences. The first difference is in step 2 in Fig. 2 and is explicitly shown in the flowchart: step 2a of receiver-side decomposition for separation of P- and S-phases is now exchanged for step 2b of suppression of surface waves. Ambient noise is often dominated by surface waves, due to the prevalence of sources at or near the surface. Each source at the surface and in-line with the two receivers (Fig. 1) contributes in phase to the retrieval of surface waves, while only a small subset of the subsurface sources contributes in phase to the retrieval of a specific body-wave reflection. Hence, using panels with surface waves in the processing (Fig. 2) leads to an overrepresentation of surface waves in the retrieved response. Because of this, processing flow for retrieval of reflections from noise must include at the beginning suppression of surface waves, rather than at the end. The suppression can be achieved in different ways. Draganov et al. (2009, 2013) suppress the surface waves using groups of geophones. The advantage of utilization of groups is that one can choose from the beginning the reject band for the surface waves. In the two mentioned articles, the used groups were tuned to suppress surface waves in the frequencies of interest for seismic exploration. Outside the reject band of the geophone groups, the surface waves remain dominant, so the authors apply frequency filtering to the data to leave only frequencies inside the reject band of the groups. In such a way, they obtained noise records with body-wave noise peaking at 10 Hz. Ruigrok et al. (2011) suppressed surface waves by searching for time windows and frequency bands, for which the body-wave energy is dominant in the noise. In their case, the band [0.4–1.0] Hz was nearly constantly dominated by body waves, while the band [0.09–0.5] Hz was sometimes dominated by body-wave energy. Zhan et al. (2010) suppressed the surface waves by choosing specific distances between the stations. As they targeted to retrieve Moho-reflected S-wave phases (SmS), they used station distances near the critical distance for SmS, because at such distances this phase becomes comparable in amplitude to the amplitudes of the surface waves. The authors retrieved reflections between 0.1 and 1 Hz.

The second difference in the processing flow is not explicitly stated in Fig. 2, as it involves an implementation of the energy normalization in step 3 in the flowchart. As the noise sources or the local seismicity might be quite close to the receiver array, some of the receivers might exhibit recordings with

DOI 10.1007/978-3-642-36197-5_378-1

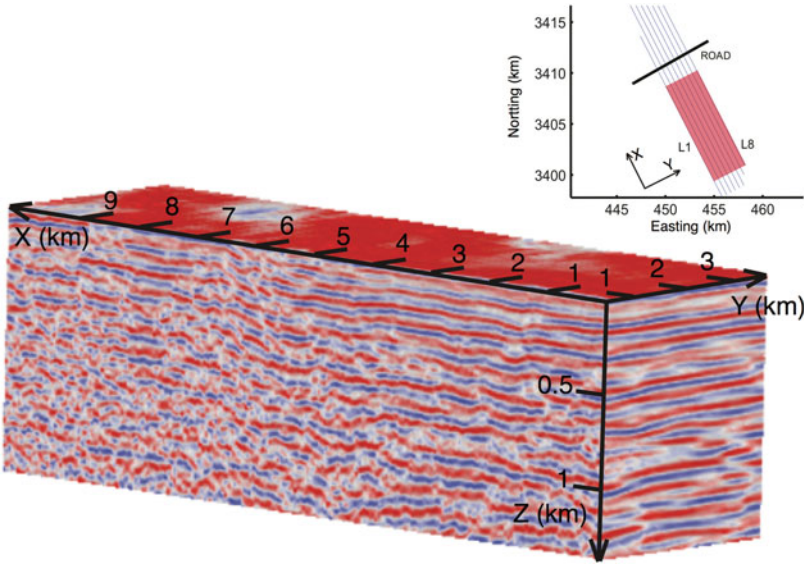

Fig. 4 Pseudo-3D image of the subsurface below the receiver lines (the *inset*) used to record about 11 h of ambient noise close to the town of Ajdabiya, Libya. The image is obtained using retrieved common-source gathers for virtual sources inside the red-highlighted part of the receiver lines, as indicated in the *inset*. This image is obtained using the line results from Draganov et al. (2013)

much higher energy than others even in the same noise panel. For this reason, the energy normalization in case of noise recordings is applied per trace per noise panel.

The subsequent processing steps for the retrieval of reflections from the ambient noise are the same as when using distant seismicity.

The illumination characteristics of the noise can also be used to suppress the surface-wave noise. The illumination information shows at which time periods body-wave noise dominates the recordings. Draganov et al. (2013) utilized this information and selected for the following correlation step only those noise panels that contained identifiable body-wave noise. This helped the authors to improve the signal-to-noise ratio of their subsurface image. The subsurface image obtained from the noise is shown in Fig. 4. The authors used about 11 h of ambient noise recorded near the town of Ajdabiya, Libya. The noise was recorded along eight lines and stored in nearly 900 noise panels of 47-s duration. Each line consisted of around 400 receiver stations. From the total number of noise panels, about 80 panels contained identifiable body-wave noise. These were used to retrieve reflection common-source gathers, which in turn were used to obtain 2D images of the subsurface. The large distance between the receiver lines precluded the authors in this case from retrieving the reflection response between the receivers at different lines. Because of this, the pseudo-3D image in Fig. 4 was obtained by interpolating the 2D images obtained below each line.

Panea et al. (2014) performed illumination analysis on the correlated noise panels. For this, the authors used the events in the correlated panels that pass through the position of the virtual source at time 0 s (Almagro Vidal et al. 2014). These events characterize the dominant event in the noise panels; the dominant event's slowness is used to conclude if the dominant event is a surface wave or a body wave. The slowness information is then also used to select for the following summation (step 8 in Fig. 2) only those correlated noise panels, which are dominated by body-wave noise. This processing resulted in better-retrieved subsurface information. The obtained image of the subsurface is shown in Fig. 5a (the narrow rectangle with red borders), where it is overlaid on an image of the subsurface obtained from an exploration survey using artificial seismic sources at the surface. The noise was recorded near the town of Mizil, Romania. The total duration of the recorded noise was about 5.5 h and was stored in about 1200

DOI 10.1007/978-3-642-36197-5_378-1

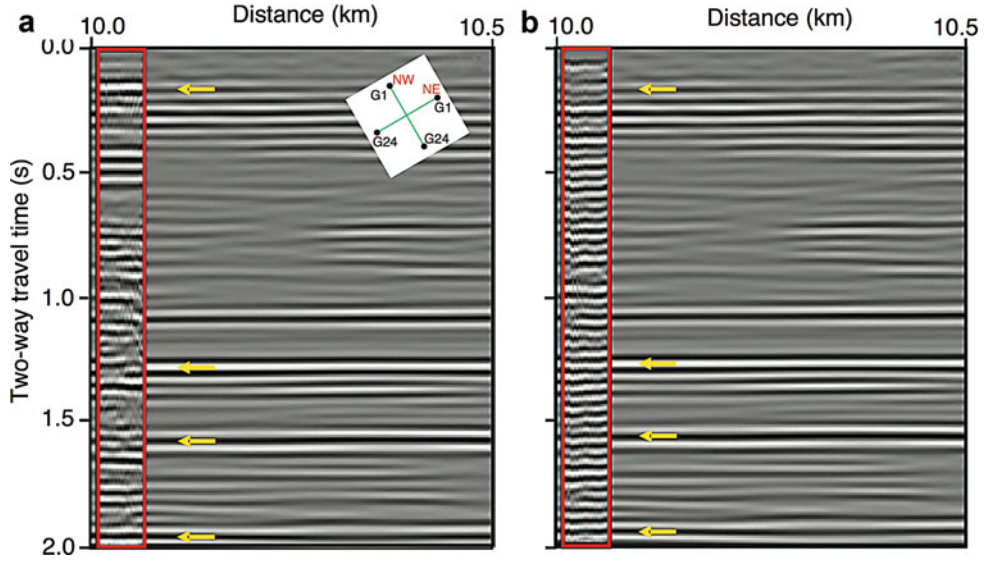

Fig. 5 (**a**) Image of the subsurface below one of the receiver lines (*the red rectangle*) of the receiver array used to record about 5.5 h of ambient noise close to the town of Mizil, Romania. (**b**) As in (**a**), but after processing additionally about 4 h of ambient noise, used together with the processed noise for (**a**). The images are obtained using retrieved common-source gathers for virtual sources along the complete receiver line. The *yellow pointers* indicate imaged geological markers in the area. The *inset* shows the orientation and geometry of the receiver array (Adapted from Panea et al. (2014))

noise panels of 16-s length. The recording array consisted of two perpendicular lines, each with 24 receivers separated by 2.5 m. From these panels, 720 showed to be dominated by body-wave noise (inside the chosen frequency band of 11–23 Hz) and used to obtain the image in Fig. 5a. Figure 5b illustrates the result of using more recorded noise. This image is obtained by processing together the noise used to obtain Fig. 5a with extra ambient noise of about 4 h recorded at later time. The image in Fig. 5b shows better correlation with reflectors in the artificial-source seismic section, including the known geological markers (indicated by the pointers). The improvement comes from extra illumination directions that the later ambient noise recording adds to the earlier ambient noise recording.

Ruigrok et al. (2011) used an array of receivers in the Abu Gharadig basin, Egypt. In-line interstation spacing was 500 m, with a more densely sampled (350 m) area in the middle of the array. In total, about 60 h of noise were simultaneously recorded on all 110 stations. Noise from a variety of sources was detected. Below 0.5 Hz, most of the energy was caused by swell interactions on distant oceans; between 0.5 and 1.0 Hz, most of the noise originated from wind-sea interactions at the Mediterranean Sea; above 1.0 Hz, most of the noise was caused by anthropogenic activity.

The recording was split up in different frequency bands, to separate different noise phenomena. Illumination analysis was performed by beamforming time windows of noise. The beamforming analysis shows whether a time window is dominated by a waveform from a certain direction (back azimuth) and apparent velocity (inverse of ray parameter).

In the frequency band [0.4–1.0] Hz, a large part of the time windows was found to be dominated by ray parameters that correspond to body waves and was further processed (steps 3–9 in Fig. 2). For a linear subarray (Fig. 6a), only time windows were used which were dominated by back azimuths that are close to the orientation of this subarray. The obtained reflection responses were sorted to common-midpoint gathers. Figure 6b shows the gather for a midpoint in the center of the subarray. The solid black lines bound the range for which kinematically correct reflections were expected to be estimated with the used illumination range. The dashed lines show the expected timing for a P- and S-wave reflection from the basin-basement interface. Vertical particle-velocity recordings, dominated by small ray parameters, were

DOI 10.1007/978-3-642-36197-5_378-1

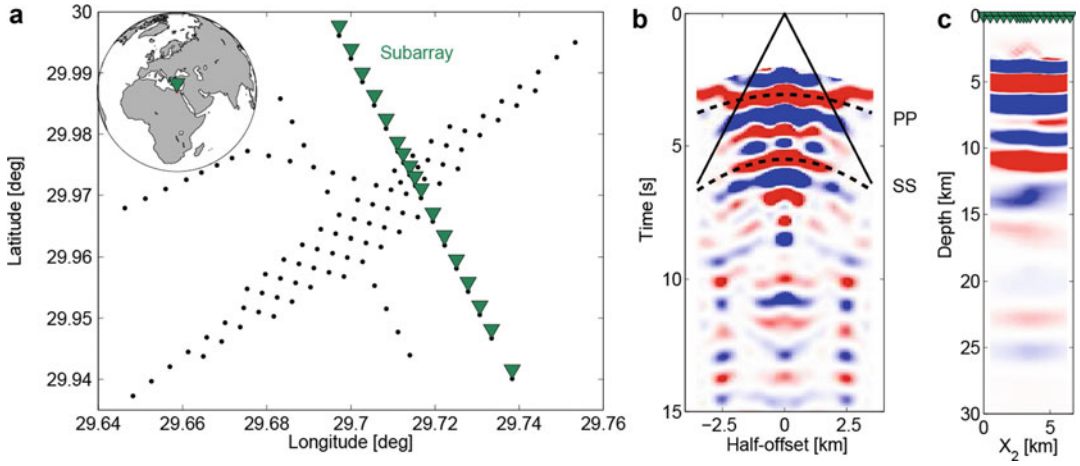

Fig. 6 (**a**) The layout of the Egypt array (*black dots*), with one subarray highlighted (*green triangles*). In the *inset*, the location of the array is shown with a *green triangle*. (**b**) Retrieved reflection responses for the subarray, in the frequency band [0.4–1.0] Hz, sorted to a common-midpoint gather. (**c**) Migrated image showing the main reflector below the subarray (at ∼5-km depth). On (**b**) and (**c**), *red* and *blue* denote positive and negative amplitudes, respectively. The effective wavelet is similar to a Ricker wavelet. Hence, a sudden increase in seismic impedance with depth is imaged by *red* with blue side lobes on either side (Adapted from Ruigrok et al. (2011))

used as an input to the processing. However, no explicit S-wave removal was applied. As a consequence, the reflection response contains both P- and S-wave reflections. Figure 6c shows the reflection image obtained by migrating the retrieved reflection responses using P-wave velocities. This image shows clearly the basin-basement interface at ∼5-km depth and a nonphysical reflector at ∼11-km depth, which is due to migrating the S-wave reflections from the basin-basement interface with P-wave velocities. This analysis shows that the basin-basement interface is nearly flat below the subarray.

Summary

High-resolution images of the subsurface are obtained using reflection seismics with artificial sources. But utilization of artificial sources is not always possible. Instead, recordings from passive sources can be used. An explanation was given on how seismic interferometry by cross-correlation can be applied to passive recordings to retrieve reflection information of the subsurface as if from artificial sources at the positions of receivers. A processing flow was described on how to obtain virtual common-source gathers, which were then used to obtain images of the subsurface. In the processing, a distinction was made for measurements from distant sources, on the one hand, and noise and local seismicity measurements, on the other hand. Examples showed obtained images of the subsurface at local and regional scales from ambient noise and from distant seismicity.

Cross-References

- ▶ Ambient Noise
- ▶ Artificial Source
- ▶ Coda Wave
- ▶ Free Surface
- ▶ Green's Function

DOI 10.1007/978-3-642-36197-5_378-1

- Microseisms
- Moho Discontinuity
- Quality Factor
- Ray Parameter
- Specular Ray
- Stationary Phase
- Teleseismic

References

Abe S, Kurashimo E, Sato H, Hirata N, Iwasaki T, Kawanaka T (2007) Interferometric seismic imaging of crustal structure using scattered teleseismic waves. Geophys Res Lett 34:L19305. doi:10.1029/2007GL030633

Almagro Vidal C, Draganov D, van der Neut J, Drijkoningen G, Wapenaar K (2014) Retrieval of reflections from ambient-noise field data using illumination diagnosis. Geophys J Int 198:1572–1584. doi:10.1093/gji/ggu164

Campillo M, Paul A (2003) Long-range correlations in the diffuse seismic coda. Science 299:547–549

Claerbout JF (1968) Synthesis of a layered medium from its acoustic transmission response. Geophysics 33:264–269

Daneshvar MR, Clarence CS, Savage MK (1995) Passive seismic imaging using microearthquakes. Geophysics 60:1178–1186

Draganov D, Campman X, Thorbecke J, Verdel A, Wapenaar K (2009) Reflection images from ambient seismic noise. Geophysics 74:A63–A67. doi:10.1190/1.3193529

Draganov D, Ghose R, Ruigrok E, Thorbecke J, Wapenaar K (2010) Seismic interferometry, intrinsic losses and Q-estimation. Geophys Prospect 58:361–373. doi:10.1111/j.1365-2478.2009.00828.x

Draganov D, Heller K, Ghose R (2012) Monitoring CO2 storage using ghost reflections retrieved from seismic interferometry. Int J Greenh Gas Con 11S:S35–S46. doi:10.1016/j.ijggc.2012.07.026

Draganov D, Campman X, Thorbecke J, Verdel A, Wapenaar K (2013) Seismic exploration-scale velocities and structure from ambient-seismic noise (>1 Hz). J Geophys Res 118:1–16. doi:10.1002/jgrb.50339

Duvall T, Jeffferies S, Harvey J, Pomerantz A (1993) Time–distance helioseismology. Nature 362:430–432

Frank JG, Ruigrok EN, Wapenaar K (2014) Shear wave seismic interferometry for lithospheric imaging: application to southern Mexico. J Geophys Res: Solid Earth 119:5713–5726. doi:10.1002/2013JB010692

Kennett B (1991) The removal of free surface interactions from three-component seismograms. Geophys J Int 104:153–163

King S, Curtis A (2012) Suppressing nonphysical reflections in Green's function estimates using source-receiver interferometry. Geophysics 77:Q15–Q25. doi:10.1190/GEO2011-0300.1

Nakata N, Snieder R, Tsuji T, Larner K, Matsuoka T (2011) Shear-wave imaging from traffic noise using seismic interferometry by cross-coherence. Geophysics 76:SA97–SA106. doi:10.1190/GEO2010-0188.1

Nakata N, Snieder R, Behm M (2014) Body-wave interferometry using regional earthquakes with multidimensional deconvolution after wavefield decomposition at free surface. Geophys J Int 199:1125–1137. doi:10.1093/gji/ggu316

Panea I, Draganov D, Almagro Vidal C, Mocanu V (2014) Retrieval of reflections from ambient noise recorded in Mizil area, Romania. Geophysics 79:Q31–Q42. doi:10.1190/GEO2013-0292.1

Ruigrok E, Wapenaar K (2012) Global-phase seismic interferometry unveils P-wave reflectivity below the Himalayas and Tibet. Geophys Res Lett 39, L11303. doi:10.1029/2012GL051672

Ruigrok E, Campman X, Draganov D, Wapenaar K (2010) High-resolution lithospheric imaging with seismic interferometry. Geophys J Int 183:339–357. doi:10.1111/j.1365-246X.2010.04724.x

Ruigrok E, Campman X, Wapenaar K (2011) Extraction of P-wave reflections from microseisms. Comptes Rendus Geoscience 343:512–525. doi:10.1016/j.crte.2011.02.006

Scherbaum F (1987) Seismic imaging of the site response using microearthquake recordings, Part II – application to the Swabian Jura, southwest Germany, seismic network. Bull Seismol Soc Am 77:1924–1944

Schuster GT (2009) Seismic interferometry. Cambridge University Press, Cambridge

Schuster GT, Yu J, Rickett J (2004) Interferometric/daylight seismic imaging. Geophys J Int 157:838–852

Shapiro NM, Campillo M (2004) Emergence of broadband Rayleigh waves from correlations of the ambient seismic noise. Geophys Res Lett 31:L07614

Snieder R (2004) Extracting the Green's function from the correlation of coda waves: a derivation based on stationary phase. Phys Rev E 69:046610. doi:10.1103/PhysRevE.69.046610

Snieder R, Wapenaar K, Larner K (2006) Spurious multiples in seismic interferometry of primaries. Geophysics 71:SI111–SI124. doi:10.1190/1.2211507

Wapenaar K (2004) Retrieving the elastodynamic Green's function of an arbitrary inhomogeneous medium by cross correlation. Phys Rev Lett 93:254301. doi:10.1103/PhysRevLett.93.254301

Wapenaar K, Fokkema J (2006) Green's function representations for seismic interferometry. Geophysics 71:SI33–SI46. doi:10.1190/1.2213955

Wapenaar K, Draganov D, Robertsson JOA (eds) (2008) Seismic interferometry: history and present status. Society of Exploration Geophysicists, Tulsa

Yilmaz O (1999) Seismic data processing, 9th edn. Society of Exploration Geophysicists, Tulsa

Zhan Z, Ni S, Helmberger D V, Clayton R W (2010) Retrieval of Moho-reflected shear wave arrivals from ambient seismic noise. Geophys J Int 182:408-420. doi:10.1111/j.1365-246X.2010.04625.x.